ICONHIC2019
2nd International Conference on Natural Hazards & Infrastructure
23-26 June, 2019, Chania, Greece

Modelling the Seismic Soil-Structure Interaction for Wind Turbines Using Simple Physical Models

F. Taddei[1], A. Greim, H. Englert, G. Müller
Chair of Structural Mechanics, Technical University of Munich

ABSTRACT

The dynamic interaction between the structure, the foundation and the underlying soil has a relevant influence on the global dynamic behavior of wind turbines and can affect its functionality. The Soil-Structure Interaction (SSI) effects can be estimated with numerical models. As in many other application of civil engineering, the simulation of tower-like buildings can be conducted by means of idealized one-dimensional dynamic systems. Usually, these structures are modeled as cantilever beam elements, fixed at the base. However, it is important to include the effects of the elastic soil on the dynamic response of wind turbines in the modeling process, keeping the computational time affordable and the model reliable. In this contribution, we present a practical semi-analytical model for the estimation of the SSI response of wind turbines in the frequency domain. We show a validation of the implementation in *Matlab* through benchmark problems. Finally, we demonstrate its use analyzing the influence of soil stiffness, soil layering, foundation embedment and variations in the seismic input on the seismic response of wind turbines.

Keywords: soil-structure interaction, seismic analysis, truncated cone model, Euler-Bernoulli beam

INTRODUCTION

Soil-structure interaction (SSI) analyses assess the interplay of two coupled systems: the structure and its underlying soil. In general, these two systems are connected to each other through the foundations. Due to SSI effects the response of a building-soil system differs from the response of the building rigidly constrained at its base. The latter case is a purely theoretical condition and does not exist in reality, but is commonly assumed in practice.

The SSI leads to two main effects: 1) kinematic interaction, that is the SSI causes the input motions to deviate from the free-field motions due to the presence of a rigid foundation, 2) inertial interaction between structure and soil. It is important to stress that these two aspects can act in opposite directions and it is not possible to establish deductively whether the dynamic response of the structure will be adversely or beneficially influenced. For each specific configuration of wind turbine and underlying soil an exhaustive investigation is necessary.

Several methods for the SSI analysis have been proposed and successfully applied to wind turbines *(Schauer & Rodriguez, 2018; Schauer, Taddei, & Morawietz, 2018; Taddei, Butenweg, & Klinkel, 2015; Taddei, Schauer, & Meinerzhagen, 2017)*. In these previous studies it was demonstrated that soil-structure interaction issues are particularly important for the exact estimation of the seismic response of wind turbines, leading to more reliable performance assessments and costs estimations.

[1] Corresponding Author: F. Taddei, *Technical University of Munich, Francesca.taddei@tum.de*

In this contribution, we propose an alternative to three dimensional complex numerical methods for SSI analyses, which can be used for fast parametric studies. This method is developed in the frequency domain and thus restricted to the case of linear systems.

The soil sub-model is based on previous developments of (*Wolf & Deeks, 2004*) which simulate the propagation of waves into an infinite medium similarly to a tapered bar with its cross area increasing along the axis. Embedded foundations with quite arbitrary shapes in layered soil deposits underlain by either a rigid base or an infinite half space can be addressed.
The sub-model for the wind turbine tower is based on 1-D Euler-Bernoulli assumptions. Seismic loads as well as external loads due to aerodynamics, wind and water waves can be applied to the model.
Several application of the soil cones models can be found in literature, such as in (*Butenweg, Rosin, & Holler, 2017; Harte & Basu, 2013; Harte, Basu, & Nielsen, 2012; Mohasseb & Abdollahi, 2009*), where it is demonstrated that they provide enough accuracy for typical engineering applications.

The salient properties of this model are:

- the structure is represented by an analytical 1-D Euler-Bernoulli beam with a constant distributed mass and bending stiffness, as described by *(Koloušek & McLean, 1973)*
- the soil is represented by a truncated cone model, as described by *(Wolf & Deeks, 2004)*
- the foundation is represented by rigid disks on the surface or embedded in the soil, as described by *(Wolf & Deeks, 2004)*;
- the seismic loads take into account the amplification effects of the site and can be applied at different levels, as described in *(Wolf & Deeks, 2004)*.

The proposed model is thought for practitioners, to develop their own SSI model. Of particular interest is the extension of the *Matlab* program CONAN *(Wolf & Deeks, 2004)*, which includes the developed features and provides a starting point for custom-designed solutions.

METHODS

Soil model: cone models
The cone models after *(Wolf & Deeks, 2004)* simulate the propagation of waves into an infinite medium similarly to a tapered bar with its cross section area increasing along the bar axis. The area of the cone increases in the direction of the wave propagation representing the spreading of the disturbance in a medium. Thus, the cones (or cone segments) are 'radiating' and fulfill the radiation condition. If the soil is layered, several physical cones are combined in series to account for reflection and refraction at the interface between layers.

The foundation is placed on the top of the cone series or is embedded into the soil. The waves propagate in outward direction from the foundation, get reflected at the fixed boundary. At the free surface, the waves propagate in their own cones. The embedded foundation is modelled with a stack of disks in that part of the soil which will be excavated, with the actual layers subdivided into fictitious layers of thickness d. In order to ensure a correct wave propagation, the fictitious thickness must be chosen such that $d < \frac{\pi c}{5\omega}$ holds, where ω represents the loading circular frequency and c designates the appropriate wave velocity for the considered seismic motion, either c_s for S-waves or c_p for P-waves. In this contribution we focus on vertically propagating S-waves, where the particle motion is only in horizontal direction, since this motion appears to be the most relevant for wind turbines.

Using the cone models, the free field motion u_f results from the amplification of the seismic signal defined at the outcrop, also called 'control motion' u_c. This is sketched on the left part of Figure 1. In absence of a foundation embedment, the free field motion u_f coincides with the foundation input motion u_0^g. When the foundation is embedded, the kinematic interaction between the soil and the foundation leads to a discrepancy between the free field motion u_f and the foundation input motion u_0^g. These aspects are accounted for in the computation of the dynamic soil stiffness. In more detail, the dynamic flexibility of the free field with respect to the relevant degrees of freedom of the rigid foundation (right part of Figure 1) is established addressing the wave pattern in the layered half space. The inversion of this relationship, an enforcement of the rigid body motion of the foundation, and the excavation of the trapped material yield the dynamic-stiffness coefficients of the embedded foundation and the effective foundation input motion u_0^g *(Wolf & Deeks, 2004)*.

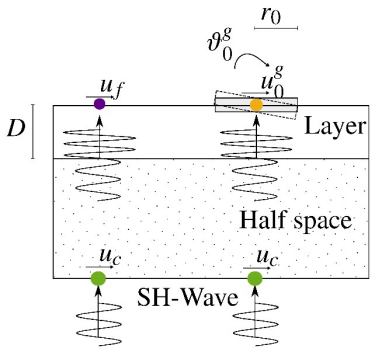

Figure 1. Sketch of the wave amplification effect for a vertically-propagating horizontal S-wave: on the left, without the presence of the structure (free field) and, on the right, including the rigid foundation with the relevant degrees of freedom activated by the S-wave

In the following we briefly recall the basics of the cone model after *(Wolf & Deeks, 2004)*. Assuming the case of a disk of radius r_0, embedded into a homogeneous half-space with shear modulus G_s , Poisson's ratio ν_s , mass density ρ_s and hysteretic damping ratio ξ_s , modelled as a (one-sided) truncated semi-infinite cone with the same material properties as the half-space. To introduce hysteretic material damping, the real shear modulus is multiplied by $(1 + 2i\xi_s)$. The relationship between the amplitudes of the horizontal load $Q_0(\omega)$ and moment $R_0(\omega)$, applied to the disk, and the coupled horizontal and rocking motions of the disk with amplitude $u_0(\omega)$ and $\vartheta_0(\omega)$ is:

$$\begin{bmatrix} Q_0(\omega) \\ R_0(\omega) \end{bmatrix} = \left[\mathbf{A}^T \begin{bmatrix} \mathbf{S}^f(\omega) & 0 \\ 0 & \mathbf{S}_\vartheta^f(\omega) \end{bmatrix} \mathbf{A} + \omega^2 \mathbf{M} \right] \begin{bmatrix} u_0(\omega) \\ \vartheta_0(\omega) \end{bmatrix} \tag{1}$$

where $\mathbf{S}^f(\omega)$ and $\mathbf{S}_\vartheta^f(\omega)$ are the dynamic stiffness coefficients of the soil, for the horizontal and rocking motion respectively, without foundation and excavated part (free field), $\mathbf{A}$ is the kinematic-constraint matrix with values 1 (or equal to the distances between the disks and the tower base) or 0 for the rigid body motion of the foundation, and $\mathbf{M}$ is the trapped mass matrix for the rigid body motion of the excavated part of the soil. For conciseness, Equation 1 rewrites:

$$\begin{bmatrix} Q_0(\omega) \\ R_0(\omega) \end{bmatrix} = \underbrace{\begin{bmatrix} \mathbf{S}_h(\omega) & \mathbf{S}_{hr}(\omega) \\ \mathbf{S}_{hr}(\omega) & \mathbf{S}_r(\omega) \end{bmatrix}}_{\mathbf{S}_{00}^g(\omega)} \begin{bmatrix} u_0(\omega) \\ \vartheta_0(\omega) \end{bmatrix} \tag{2}$$

where $\mathbf{S}_{00}^g(\omega)$ is the dynamic-stiffness matrix of the embedded foundation. The effective foundation input motion consists of an averaged horizontal component and a rocking component with amplitudes:

$$\begin{bmatrix} u_0^g(\omega) \\ \vartheta_0^g(\omega) \end{bmatrix} = \mathbf{S}_{00}^g(\omega)^{-1} \mathbf{A}^T \begin{bmatrix} \mathbf{S}^f(\omega)\mathbf{u}^f(\omega) \\ 0 \end{bmatrix} \tag{3}$$

The free-field displacements $\mathbf{u}^f(\omega)$ are to be determined at the locations of the subdisks for the vertically propagating S-waves (and possibly also for P-waves in case of a vertical earthquake). The spectral amplitude of the control motion $u_c(\omega)$ can be defined either at the free surface of the site, or at an assumed fictitious rock outcrop.

Tower model: Kolousek functions

(Koloušek & McLean, 1973) gave the analytical solutions for a continuous prismatic Euler-Bernoulli-beam with different boundary conditions subjected to harmonic loads. These solutions establish the relationship between forces and displacements at the beam ends, as shown in Figure 2b. They are exact for the case of loads applied at the beam ends and are expressed in terms of sinusoidal and hyperbolic sinusoidal functions. Thus, the derivation of the exact dynamic stiffness matrix of the structure is straightforward.

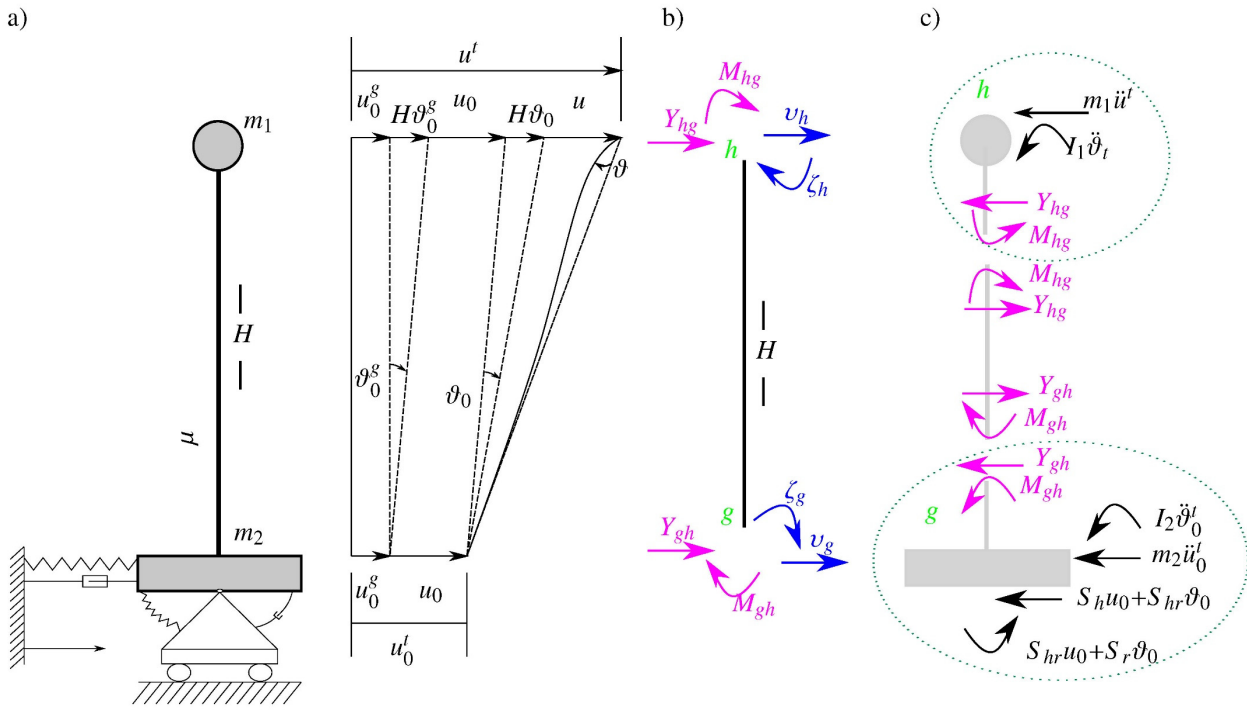

Figure 2. a) Model b) Exact forces and displacements at the ends of the beam after the convention of *(Kolouˇsek & McLean, 1973)* c) External and internal nodal forces

For the element described in Figure 2b, the relationship between forces and displacement at the beam ends reads as in Equation 4:

$$\begin{aligned} Y_{gh} &= \frac{EI}{H}\left[\frac{F_6(\lambda)}{H^2}v_g - \frac{F_4(\lambda)}{H}\zeta_g + \frac{F_5(\lambda)}{H^2}v_h + \frac{F_3(\lambda)}{H}\zeta_h\right] \\ M_{gh} &= \frac{EI}{H}\left[-\frac{F_4(\lambda)}{H}v_g + F_2(\lambda)\zeta_g - \frac{F_3(\lambda)}{H}v_h + F_1(\lambda)\zeta_h\right] \\ Y_{hg} &= \frac{EI}{H}\left[\frac{F_5(\lambda)}{H^2}v_g - \frac{F_3(\lambda)}{H}\zeta_g + \frac{F_6(\lambda)}{H^2}v_h + \frac{F_4(\lambda)}{H}\zeta_h\right] \\ M_{hg} &= \frac{EI}{H}\left[\frac{F_3(\lambda)}{H}v_g + F_1(\lambda)\zeta_g + \frac{F_4(\lambda)}{H}v_h + F_2(\lambda)\zeta_h\right] \\ &\text{with} \quad \lambda^4 = H^4\omega^2\frac{\mu}{EI} \end{aligned} \tag{4}$$

The functions F_n depend on the parameter λ, which is related to excitation frequency ω. The complete expressions for the $F_n(\lambda)$ are shown in Annex A.
The generalized displacements at the beam ends, can be substituted with those defined in Figure 2a:

$$\begin{aligned} v_g &= u_0^g + u_0 \\ \zeta_g &= \vartheta_0^g + \vartheta_0 \\ v_h &= u_0^g + H\vartheta_0^g + u_0 + H\vartheta_0 + u \\ \zeta_h &= \vartheta_0^g + \vartheta_0 + \vartheta \end{aligned} \tag{5}$$

Setting the equilibrium of horizontal forces and moment at the node h and at both nodes $(h+g)$:

$$\begin{aligned} Y_{hg} + m_1\ddot{v}_h &= 0 \\ Y_{hg} + m_1\ddot{v}_h + Y_{gh} + m_2\ddot{v}_g + S_h u_0 + S_{hr}\vartheta_0 &= 0 \\ M_{hg} + I_1\ddot{\zeta}_h &= 0 \\ M_{hg} + M_{gh} + I_2\ddot{\zeta}_g + I_1\ddot{\zeta}_h + HY_{hg} + Hm_1\ddot{v}_h + S_{hr}u_0 + S_r\vartheta_0 &= 0 \end{aligned} \tag{6}$$

In Equation 6 we considered the loads and moments at node h (which are in equilibrium and their sum is zero) also in the equilibrium for both nodes h+g. This is cumbersome and could be improved by considering the equilibrium only at h and only at g, instead of $(h+g)$. However, here we chose this less efficient formulation, in order to follow the procedure described in *(Wolf & Deeks, 2004)*.

Substituting Equation 4, 5 and 6 and reassembling the expressions with respect of the unknown variables u_0, ϑ_0, u and ϑ in matrix form, bringing the known terms with the seismic inputs u_0^g and ϑ_0^g on the right side (the dependency on λ is omitted for clarity) leads to the SSI system of equations in Equation 7 to 11.

$$\boldsymbol{K_{SSI}C} = \boldsymbol{B} = \boldsymbol{B}_1 u_0^g + \boldsymbol{B}_2 \vartheta_0^g \tag{7}$$

$$\boldsymbol{C} = \begin{pmatrix} u \\ u_0 \\ \vartheta \\ \vartheta_0 \end{pmatrix} \tag{8}$$

$$\boldsymbol{K_{SSI}} = \frac{EI}{H^3}(\boldsymbol{K_{SSI}^1} \quad \boldsymbol{K_{SSI}^2} \quad \boldsymbol{K_{SSI}^3} \quad \boldsymbol{K_{SSI}^4})$$

$$\boldsymbol{K_{SSI}^1} = \begin{pmatrix} F_6 - \frac{H^3\omega_j^2 m_1}{EI} \\ F_5 + F_6 - \frac{H^3\omega_j^2 m_1}{EI} \\ HF_4 \\ H(-F_3 + F_4 + F_6) - \frac{H^4\omega_j^2 m_1}{EI} \end{pmatrix}; \quad \boldsymbol{K_{SSI}^2} = \begin{pmatrix} F_5 + F_6 - \frac{H^3\omega_j^2 m_1}{EI} \\ 2F_5 + 2F_6 - \frac{H^3\omega_j^2(m_1+m_2)}{EI} + \frac{H^3 S_h}{EI} \\ H(F_4 + F_3) \\ H(F_5 + F_6) - \frac{H^4\omega_j^2 m_1}{EI} + \frac{H^3 S_{hr}}{EI} \end{pmatrix}$$

$$\boldsymbol{K_{SSI}^3} = \begin{pmatrix} HF_4 \\ H(F_4 + F_3) \\ H^2F_2 - \frac{H^3 I_1 \omega_j^2}{EI} \\ H^2(F_1 + F_2 + F_4) - \frac{H^3 I_1 \omega_j^2}{EI} \end{pmatrix}; \tag{9}$$

$$\boldsymbol{K_{SSI}^4} = \begin{pmatrix} H(-F_3 + F_4 + F_6) - \frac{H^4\omega_j^2 m_1}{EI} \\ H(F_5 + F_6) - \frac{H^4\omega_j^2 m_1}{EI} + \frac{H^3 S_{hr}}{EI} \\ H^2(F_1 + F_2 + F_4) - \frac{H^3 I_1 \omega_j^2}{EI} \\ H^2(2F_1 + 2F_2 - 2F_3 + 2F_4 + F_6) + \frac{H^3\omega_j^2(-I_1 - I_2 - H^2 m_1)}{EI} + \frac{H^3 S_r}{EI} \end{pmatrix}$$

$$\boldsymbol{B}_1 = \frac{EI}{H^3}\begin{pmatrix} -F_5 - F_6 + \frac{H^3\omega_j^2 m_1}{EI} \\ -2F_5 - 2F_6 + \frac{H^3\omega_j^2(m_1+m_2)}{EI} \\ -H(F_3 + F_4) \\ H(-F_5 - F_6) + \frac{H^4\omega_j^2 m_1}{EI} \end{pmatrix} \tag{10}$$

$$\boldsymbol{B}_2 = \frac{EI}{H^2}\begin{pmatrix} F_3 - F_4 - F_6 + \dfrac{H^3 m_1 \omega_j^2}{EI} \\ -F_5 - F_6 + \dfrac{H^3 m_1 \omega_j^2}{EI} \\ -H(+F_1 + F_2 + F_4) + \dfrac{H^2 \omega_j^2 I_1}{EI} \\ H(-2F_1 - 2F_2 + 2F_3 - 2F_4 - F_6) + \dfrac{H^2 \omega_j^2 (I_1 + I_2 + H^2 m_1)}{EI} \end{pmatrix} \tag{11}$$

Equation 6 can be extended to include aerodynamic loads at the tower head or wave loads for offshore structures at the foundation level. Therefore, an extended version of the proposed method can be applied also to offshore wind turbines. Moreover, the functions F_n are only valid for a constant section along the beam axis. A tower with a variable section can be simulated approximating it with several beam elements with constant cross section and coupling them by enforcing equilibrium at the coupling nodes.

Validation

Let us consider the steady-state response of a bending beam grounded on a very stiff soil subjected to a vertically-propagating horizontal assuming a control motion $u_c(\omega)$= 0.1 m, constant throughout the frequency range and applied on a fictitious rock outcrop. The beam foundation is a circular disk with a radius equal to 1 m. There are no additional lumped masses at the top and bottom of the tower, only a distributed mass along the beam. By giving a very high value to the shear modulus of the soil, the beam can be considered fixed at its base and therefore its response must be equal to the analytical solution of a cantilever beam. Table 1 shows the natural frequency of a cantilever beam with normalized properties. Figure 3a shows the transfer functions of the relative tower head displacements $u(\omega)$ (or structural distortion) with respect to both the control motion $u_c(\omega)$ and the input motion $u_0^g(\omega)$. The two lines coincide for a stiff soil and represent the transfer functions of a cantilever beam subjected to a root point excitation $u_c(\omega)$ with fixed base conditions, validating the method for the structural part.

The validation is also confirmed in Figure 3b, which compares $u^t(\omega)$ with the total foundation motion $u_0^t(\omega)$, the input motion $u_0^g(\omega)$, the control motion $u_c(\omega)$ and the free field motion $u_f(\omega)$. All the curves except the total tower head displacements coincide with the control motion $u_c(\omega)$. Figure 3a and Figure 3b show also the resonance frequencies of the system with a stiff soil, which matches the analytical values given in Table 1.

As a second validation scenario, the frequency-domain response of the beam grounded on a resonant layer underlain by a bedrock is analyzed, where the first natural frequency of the soil f_{g1} matches the first natural frequency of the structure f_1. The properties of the layer are indicated in Table 2 as 'Resonant layer 1'. Figure 3c shows the effects of the resonant layer presence on the transfer functions $u(\omega)/u_c(\omega)$ and $u(\omega)/u_0^g(\omega)$. The displacement peck corresponding to the first natural frequency of the structure is amplified of a factor equal to ca. 10 with respect to the stiff soil case. The additional peaks f_{gn} represent the natural frequencies of the layer and are computed correctly. Figure 3d shows that, at higher frequencies, the total displacements are damped, due to the additional radiation damping of the soil. In this case, the root-point excitation $u_0^g(\omega)$ and the free field $u_f(\omega)$ coincide, due to the absence of embedment.

In the third scenario, the beam grounded on a resonant layer underlain by a bedrock is considered, where the first natural frequency of the soil f_{g1} matches the second natural frequency of the structure f_2 (Table 2 - 'Resonant layer 2'). The simulation is carried out without foundation embedment and with foundation embedment e equal to 30% of H. Figure 4a and Figure 4b show the frequency-domain response of the beam-layer system without embedment and the behavior shows a resonance at f_2 as expected. Figure 4c and Figure 4d show the effect of the embedment on the input motion $u_0^g(\omega)$, and therefore on the total displacements, which are reduced w.r.t. the case without embedment. One can observe that, when the foundation is embedded, the input motion $u_0^g(\omega)$, the control motion $u_c(\omega)$ and the free field motion $u_f(\omega)$ no longer coincide, because of the kinematic interaction.

Table 1. Natural frequency of a cantilever beam of height H, distributed mass μ, rigidity EI

n	$\frac{H}{\pi}\sqrt[4]{\frac{\mu\omega_n^2}{EI}}$	f_n [Hz]
1	0.597	0.56
2	1.494	3.51
3	2.500	9.82

Table 2. Investigated soil parameters for the validation scenarios

Stiff soil	Resonant layer 1	Resonant layer 2
$\frac{G_s}{\rho_s} \to \infty$	$\frac{G_s}{\rho_s} = (f_1 \cdot 4D)^2$	$\frac{G_s}{\rho_s} = (f_2 \cdot 4D)^2$
ν_s=0.3	ν_s=0.3	ν_s=0.3
$D \to \infty$	D=1 m	D=1 m
ξ_s=5%	ξ_s=5%	ξ_s=5%

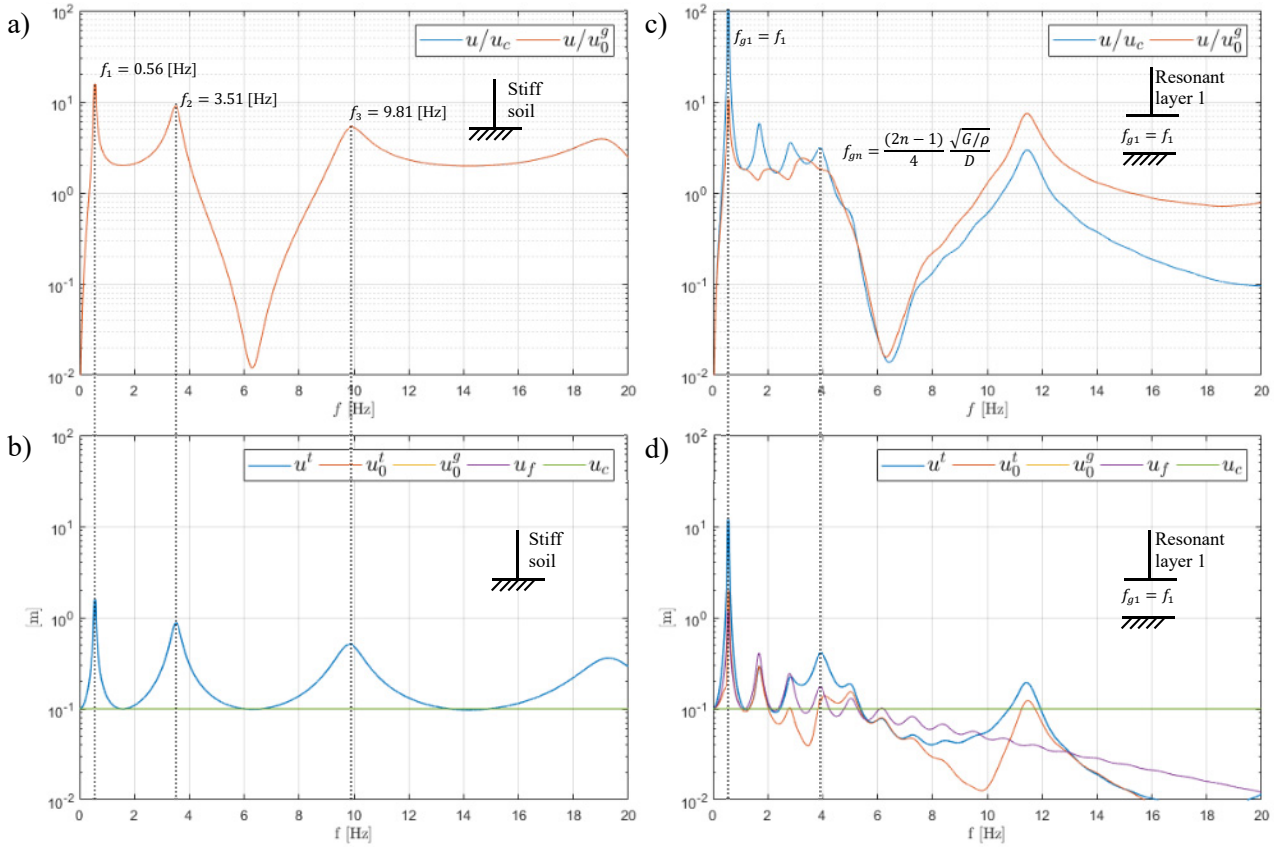

Figure 3. Validation case scenarios where the tower model parameters are normalized according to Table 2, while the soil parameters vary according to Table 2 (Resonant layer 1) in order to show the influence of a stiff soil and a resonant layer on the structural response

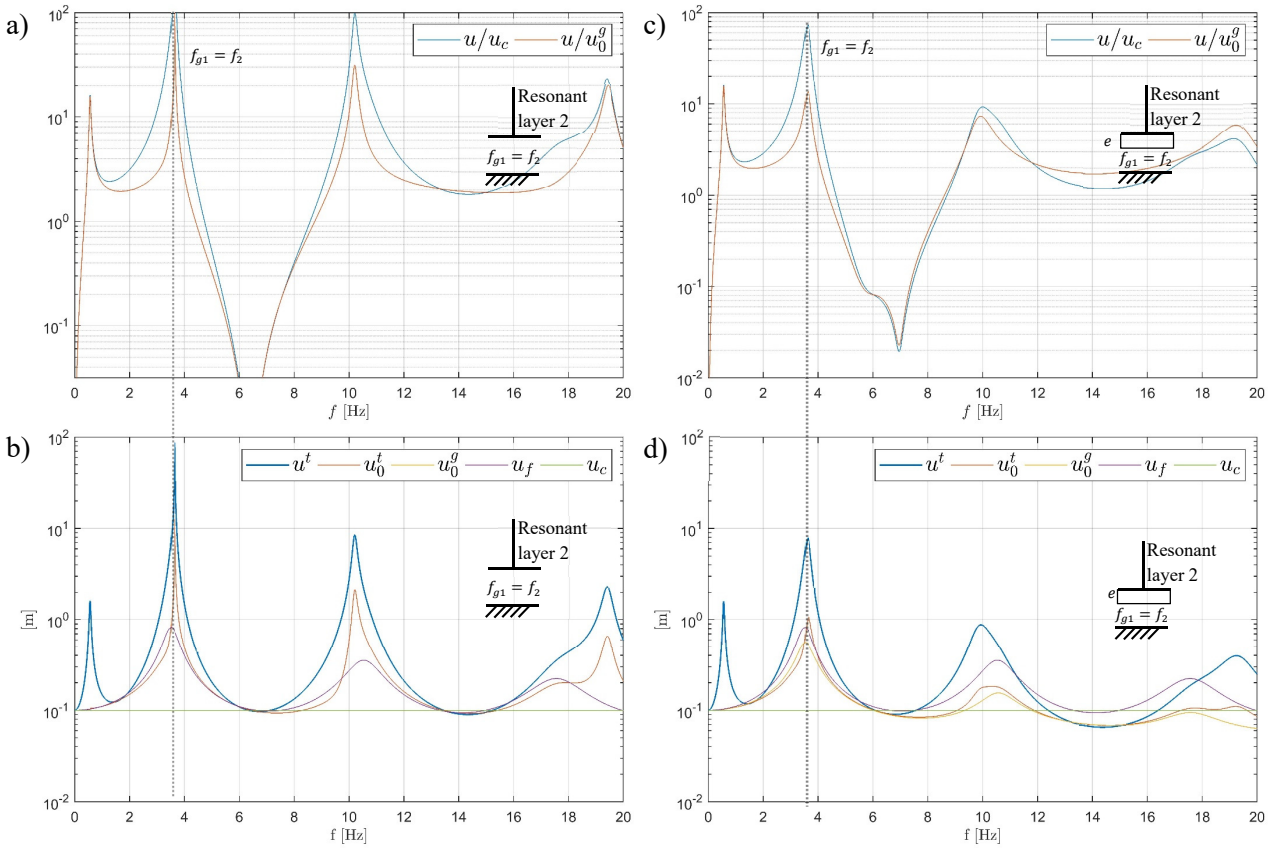

Figure 4. Validation case scenarios with the beam grounded on a resonant layer (Table 2 - 'Resonant layer 2'): transfer functions without (a, b) and with (c, d) foundation embedment. Symbols are described in Figure 1 and Figure 2a

CASE STUDY

The application of the proposed method is shown for the case of an idling 5MW onshore wind turbine subjected to different strong seismic events of Richter magnitude M>7. The two main axis of the turbine, the side-to-side and fore-aft (FA) direction are considered as uncoupled and, in this study, only the FA direction is analyzed, that is the direction perpendicular to the rotor plane. The main direction of action of the horizontal earthquake is assumed to be aligned with the FA direction. Table 3 contains the properties of tower head and foundation. The first three natural frequencies of the wind turbine, fixed at its foundation, are 0.3 Hz, 2.4 Hz and 5.6 Hz. The investigated soils are either different homogeneous half spaces with different shear moduli or different layered soils, made up of one 16m-thick layer underlain by a homogeneous half space.

Table 3. Inertial properties of tower head and foundation

E	Young's Modulus	$2.10 \cdot 10^{11}$	N/m^2
I	Average moment of inertia of the cross section	1.9	m^4
A	Average area of the cross section	0.5	m^2
H	Tower height	87,6	m
$\mu = \rho \cdot A$	Distributed mass per unit length	4551	kg/m
ξ	Damping ratio	5%	--
m_1	Lumped rotor mass	350000	kg
I_1	Lumped rotor mass moment of inertia in fore-aft direction	4.5e+7	kg/m^2
m_2	Lumped foundation mass	$772500 \cdot 10^5$	kg
I_2	Lumped foundation moment of inertia in fore-aft direction	1.13e+7	kg
r_0	Foundation radius	8	m

For all the soil profiles, the density is assumed equal to 2000 kg/m^3, the Poisson's ratio equal to 0.33, the material damping equal to 5%. The remaining soil properties are listed in Table 4. In the results, the focus lays on the relative displacements at the tower head u. However, the model provides also other important quantities such as the foundation translations and rotations, the effective input motions and the internal forces and moments according to the Euler-Bernoulli theory.

Table 4. Investigated soil profiles. $G_s^{HS}$and G_s^L are the shear moduli of the half space and of the layer respectively. c_s^L/c_s^{HS} is the layer/half space shear velocity ratio.

	homogeneous half spaces			**layered soils**		
	stiff	**medium**	**soft**	**L-stiff**	**L-medium**	**L-soft**
G_s^{HS}	$5.9 \cdot 10^8$ N/m^2	$1.5 \cdot 10^8$ N/m^2	$1.3 \cdot 10^7$ N/m^2	$8.0 \cdot 10^7$ N/m^2	$8.0 \cdot 10^7$ N/m^2	$8.0 \cdot 10^7$ N/m^2
G_s^L	--	--	--	$5.9 \cdot 10^8$ N/m^2	$1.5 \cdot 10^8$ N/m^2	$1.3 \cdot 10^7$ N/m^2
c_s^L/c_s^{HS}	--	--	--	2.7	1.3	0.4
D	--	--	--	16 m	16 m	16 m

The seismic action is modelled selecting recorded seismic strong motions with fitting characteristics for the specific analysis. The earthquake recordings were selected providing the criterion of an average shear wave velocity of the top 30 m (c_{30}) of the soil equal to 200±10m/s. Additionally, a Richter Magnitude between 7 and 8 is assumed. The selected seismic motions represent the reference control motion u_c applied on a fictitious rock outcrop:

- Chi Chi, Taiwan, 1999, M=7.62, c_{30}=199 m/s
- Darfield, New Zealand, 2010, M=7.0, c_{30}=198 m/s
- El Mayor, Cucapah, 2010, M=7.2, c_{30}=197 m/s

Influence of soil stiffness and stratification

First, the idling wind turbine coupled to three different homogeneous half spaces and subjected to the Chi Chi earthquake is investigated. The foundation is not embedded. The stiffer soil has a greater shear modulus than the soft soil, so that the shear wave velocities vary from 543 m/s to 81 m/s respectively. Figure 5a shows the transfer function for the relative displacement at the tower head for the three different half spaces. The first natural frequency of the system is less affected by the presence of the soil than the higher natural frequencies, which shift considerably towards left as the soil shear wave velocity decreases. Also the amplitudes of the displacements u are affected by the SSI and this can be clearly seen in the transient response in Figure 5c. In this case, the 'stiff' and 'medium' soils lead to very similar results, while the 'soft' soil reduces the maximum relative displacement from 0.5 m to ca. 0.35 m. Then, for the same seismic event, layered soil conditions as described in Table 4 are considered. The final results are very similar to the case of half space. After a careful comparison between the transient signals in Figure 5c and Figure 5d for the cases 'soft' and 'L-soft', one can observe a small increase of amplitude when a the soft soil becomes a layer underlain by a stiffer half space. This is due to the reflections and refractions of the waves at the interface between layer and half space, which lead to trapped energy in the layer-tower system.

Influence of embedment

Using again the seismic signal of "Chi Chi", a foundation embedment of 4 m is considered. Figure 6a shows the transfer functions for the relative displacement at the tower head with and without embedment and for fixed-base conditions. The transient response in terms of relative displacement at the tower head is affected by the presence of the embedment, which leads to a shift of the natural frequencies w.r.t. the superficial foundation and a modification of the amplitudes of the transfer functions. The presence of the embedment increases noticeably the computational time from few second to few hours.

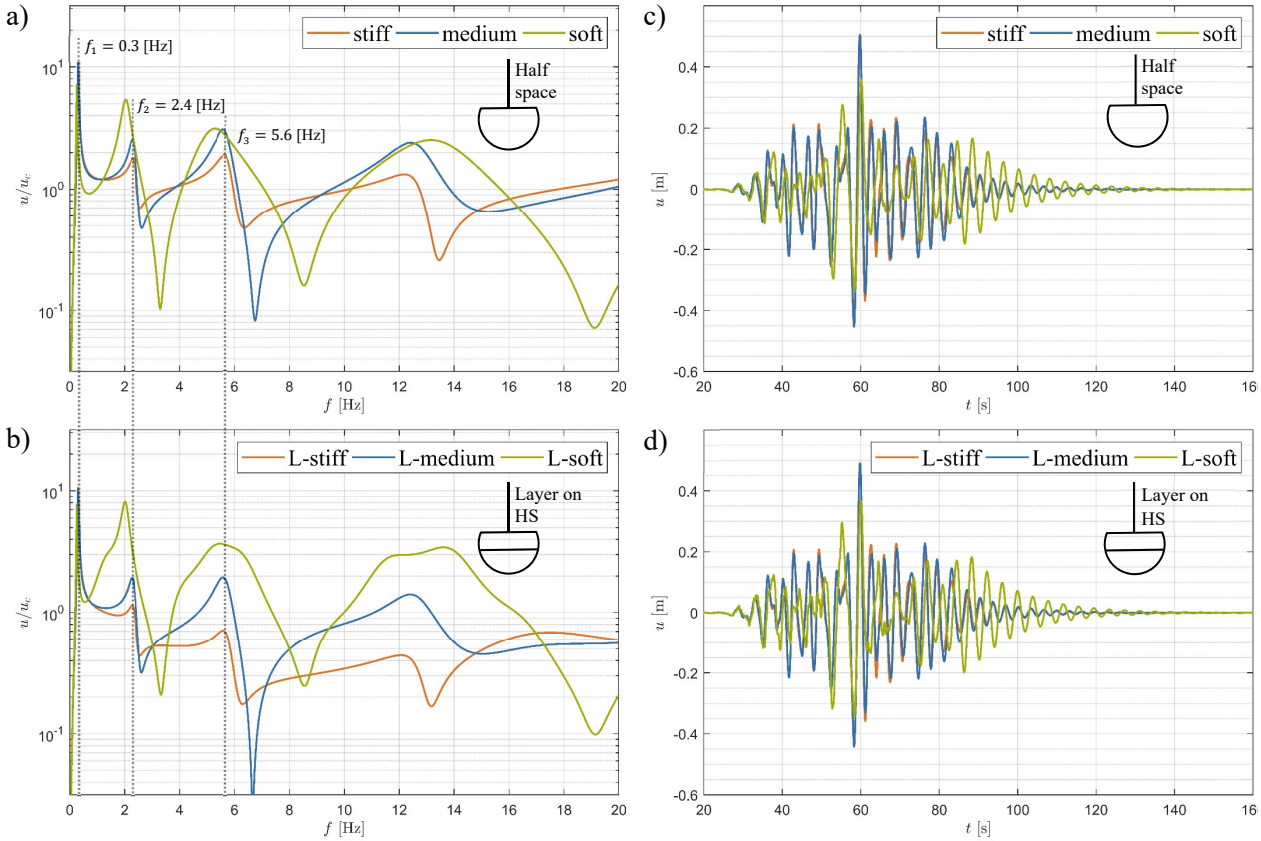

Figure 5. On the left, transfer functions for the relative displacement at the tower head for different half spaces (a) for different layered soils (b). On the right: transient response in terms of relative displacements at the tower head for different half spaces (c) for different layered soils (d)

Influence of seismic signal

Figure 7 shows the control motion in time domain $u_c(t)$ for different seismic events and the corresponding spectra $u_c(f)$ superimposed with the transfer functions u/u_c for a stiff soil and for a soft soil. First stiff-soil conditions are considered. Even if the "El Mayor" event exhibits a greater maximum absolute control motion (input) than the "Darfield" event, the latter causes a greater structural distortion u (output), as shown in Figure 7c. The spectrum of the "Darfield" event shows a higher spectral amplitude than the "El Mayor" event in correspondence with the peak of the transfer function around $f_1 = 0.3$ Hz, for stiff-soil conditions (dashed line in Figure 7b). Now, we assume soft-soil conditions. The structural distortion u for all the seismic events is reduced in amplitudes as expected according to the reduced transfer function for soft-soil conditions (dotted line in Figure 7b). However, the reduction is not the same for the different events. For example, for the "El Mayor" event, the reduced transfer function for soft-soil condition is compensated by the higher spectral amplitudes of the input in correspondence of the shifted transfer function peak for soft-soil condition. This confirms that the SSI can be both beneficial (thanks to additional damping) and disadvantageous (due to shifted natural frequencies with unexpected resonance effects or trapped energy in layered soils).

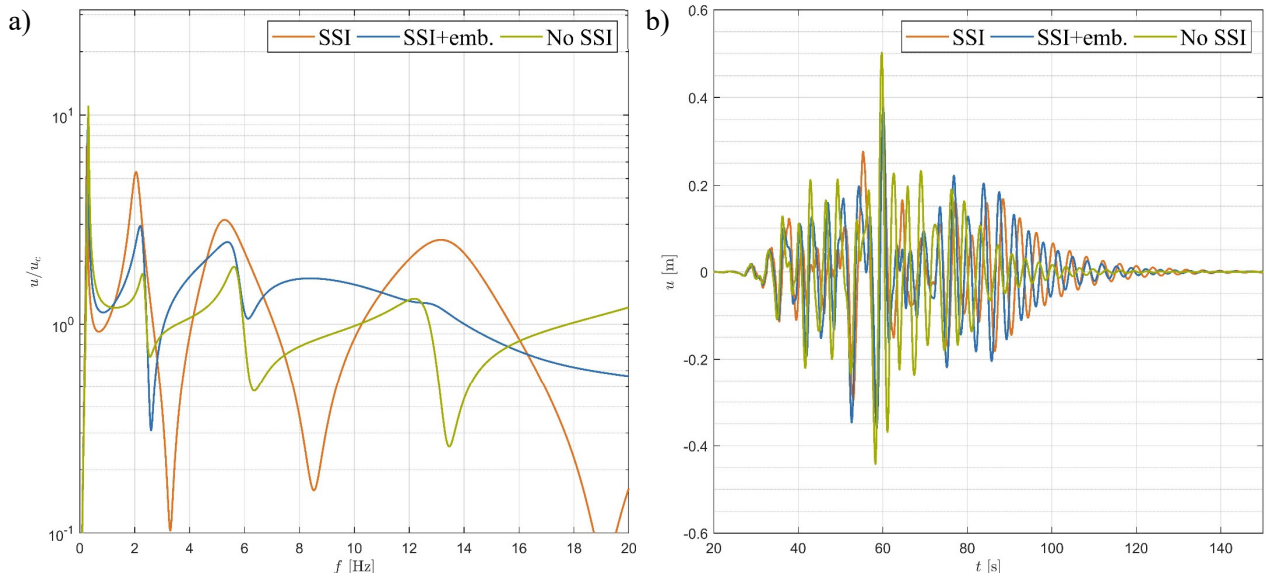

Figure 6. On the left (a): transfer functions for the relative displacement at the tower head for different soil and embedment conditions. On the right (b): transient response in terms of relative displacement at the tower head for different soil and embedment conditions

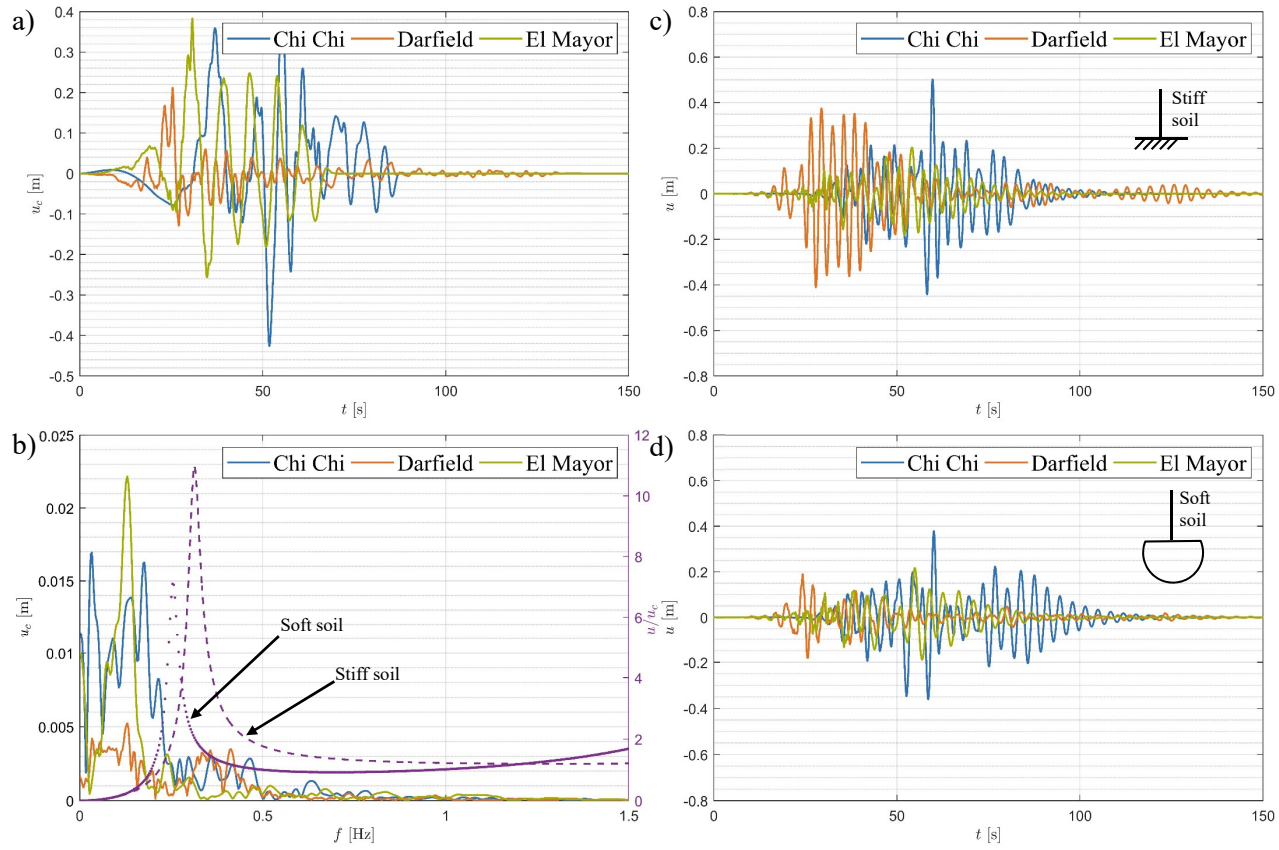

Figure 7. a) Transient signal $u_c(t)$ of the horizontal earthquake for different seismic events; b) Spectra $u_c(f)$ of the input transient signals $u_c(t)$ superimposed with the transfer functions u/u_c for a stiff soil (dashed line) and for a soft soil (dotted line), for frequency between 0 and 1.5 Hz; c) transient response in terms of relative displacement at the tower head for a stiff soil; d) transient response in terms of relative displacement at the tower head for a soft soil

CONCLUSIONS

In this contribution, we proposed a semi-analytical model for the analysis of the soil-structure interaction of wind turbines subjected to seismic loads and we checked its numerical implementation through classical benchmark problems. This model is based on the one-dimensional wave propagation theory developed in the

frequency domain and thus restricted to the case of linear systems. We presented an application of the model for the analysis of the seismic response of a 5-MW wind turbine grounded on different soils, subjected to different earthquakes, with and without SSI. We showed that the relative displacements of the tower top are affected by the presence of the soil and the effect is not always beneficial. The method can be extended for offshore wind turbines, by including external loads for the aerodynamic and hydrodynamic wave loads.

REFERENCES

Butenweg, C., Rosin, J., & Holler, S. (2017). Analysis of cylindrical granular material silos under seismic excitation. *Buildings, 7*(3), 61.

Harte, M., & Basu, B. (2013). Foundation impedance and tower transfer functions for offshore wind turbines. *Proceedings of the Institution of Mechanical Engineers, Part K: Journal of Multi-body Dynamics, 227*(2), pp. 150-161.

Harte, M., Basu, B., & Nielsen, S. R. (2012). Dynamic analysis of wind turbines including soil-structure interaction. *Engineering Structures, 45*, pp. 509-518.

Koloušek, V., & McLean, R. F. (1973). *Dynamics in engineering structures*: Butterworths.

Mohasseb, S., & Abdollahi, B. (2009). Soil-structure interaction analyses using cone models. *Journal of Seismology and Earthquake Engineering, 10*(4), pp. 167-174.

Schauer, M., & Rodriguez, G. A. R. (2018). *Seismic Transient Simulation of an Operating Wind Turbine Considering the Soil-Structure-Interaction*. Paper presented at the XIIIth International Conference on Recent Advances in Structural Dynamics, Lyon.

Schauer, M., Taddei, F., & Morawietz, S. (2018). A Strategy to Conduct Numerical Simulation of Wind Turbine Considering the Soil-Structure-Interaction by Using a Coupled FEM-SBFEM Approach in Time Domain. *IUTAM Bookseries "Symposium on Model Order Reduction of Coupled Systems (MORCOS 2018)*.

Taddei, F., Butenweg, C., & Klinkel, S. (2015). Parametric investigation of the soil–structure interaction effects on the dynamic behaviour of a shallow foundation supported wind turbine considering a layered soil. *Wind Energy, 18*(3), pp. 399-417.

Taddei, F., Schauer, M., & Meinerzhagen, L. (2017). A practical soil-structure interaction model for a wind turbine subjected to seismic loads and emergency shutdown. *Procedia engineering, 199*, pp. 2433-2438.

Wolf, J. P., & Deeks, A. J. (2004). *Foundation vibration analysis: A strength of materials approach*: Elsevier.

Annex A

Shape functions after *(Koloušek & McLean, 1973)* for a prismatic beam

$$F_1(\lambda) = -\lambda\frac{\sinh\lambda - \sin\lambda}{\cosh\lambda\cos\lambda - 1} \qquad F_2(\lambda) = -\lambda\frac{\cosh\lambda\sin\lambda - \cos\lambda\sinh\lambda}{\cosh\lambda\cos\lambda - 1}$$

$$F_3(\lambda) = -\lambda^2\frac{\cosh\lambda - \cos\lambda}{\cosh\lambda\cos\lambda - 1} \qquad F_4(\lambda) = \lambda^2\frac{\sinh\lambda\sin\lambda}{\cosh\lambda\cos\lambda - 1}$$

$$F_5(\lambda) = \lambda^3\frac{\sinh\lambda + \sin\lambda}{\cosh\lambda\cos\lambda - 1} \qquad F_6(\lambda) = -\lambda^3\frac{\cosh\lambda\sin\lambda + \cos\lambda\sinh\lambda}{\cosh\lambda\cos\lambda - 1}$$

With

$$\lambda^4 = H^4\omega^2\frac{\mu}{EI}$$